buildings

MDPI

Article

Shear Transfer in Concrete Joints with Non-Metallic Reinforcement

Lore Zierul *, Enrico Baumgärtel, David Sandmann and Steffen Marx

Institute of Concrete Structures, TUD Dresden University of Technology, 01062 Dresden, Germany
* Correspondence: lore.zierul@tu-dresden.de

Abstract: The use of non-metallic reinforcement can significantly reduce the carbon footprint of the construction sector. Mixed structures made out of steel and non-metallic reinforcement should be avoided due to the risk of galvanic corrosion. So far, researchers have been focusing on the load-bearing behavior in the longitudinal direction of the fibers. In this study, the behavior of the fibers in the non-metallic reinforcements is analyzed perpendicular to the fiber orientation. Therefore, a uniaxial shear test on a single bar (uniaxial shear test), as well as a series of push-off tests with reinforcements embedded in the concrete, was carried out. For both experiments, bars made of carbon fiber-reinforced polymers (CFRPs) and glass fiber-reinforced polymers (GFRPs) were investigated. In order to analyze the influence of non-metallic reinforcement in the joint, specimens without reinforcement have been tested as well. Also, the joint roughness and reinforcement ratio of the concrete joint was varied in the tests. The determined transverse shear strengths for the single bar exceed the values of the producer. For the push-off test, high standard deviations occurred, making it difficult to draw firm conclusions. Nevertheless, it is shown that increasing the amount of reinforcement leads to higher ultimate forces. The presented study emphasizes the necessity of further studies of the shear transfer in concrete joints.

Keywords: shear transfer; joints; carbon fiber-reinforced polymers (CFRPs); glass fiber-reinforced polymers (GFRPs); non-metallic reinforcement; carbon reinforced concrete; adhesion; friction; dowel action

check for updates

Citation: Zierul, L.; Baumgärtel, E.; Sandmann, D.; Marx, S. Shear Transfer in Concrete Joints with Non-Metallic Reinforcement. *Buildings* **2024**, *14*, 1975. https://doi.org/10.3390/buildings14071975

Academic Editors: Bo Wang, Rui Guo, Muye Yang, Weidong He and Chuntao Zhang

Received: 24 May 2024
Revised: 12 June 2024
Accepted: 24 June 2024
Published: 30 June 2024

Copyright: © 2024 by the authors. Licensee MDPI, Basel, Switzerland. This article is an open access article distributed under the terms and conditions of the Creative Commons Attribution (CC BY) license (https://creativecommons.org/licenses/by/4.0/).

1. Introduction

1.1. Motivation

The cement production is responsible for 8% of global annual CO_2 emissions [1]. To protect the steel reinforcement in order to avoid corrosion in steel-reinforced concrete, a minimum concrete cover must be maintained. The development of carbon and glass fiber-reinforced polymers is opening up new possibilities for lightweight structures. Due to its inherent corrosion resistance, high tensile strength and small weight, non-metallic reinforcement has become a promising substitute for conventional steel bars [2]. Broad research has been conducted concerning the behavior of non-metallic reinforcement in pure tensile tests, as well as experiments for non-metallic reinforcement embedded in concrete. The used reinforcement shapes varied from fibers to single yarns over to grids and bars [3–5]. According to the German DAfStb-guideline for non-metallic reinforcement published in March 2024 [6], the cross-sectional area of a non-metallic reinforcement crossing a joint must not yet be accounted for in the shear resistance. Thus, the load-bearing capacity is underestimated.

1.2. Load-Bearing Behavior in Joints

The ultimate load of a joint is reached after the mechanisms of adhesion, friction and the load-carrying action of the reinforcement are exceeded. The latter can be divided into dowel action and clamping. An overview of the described mechanisms is shown in Figure 1.

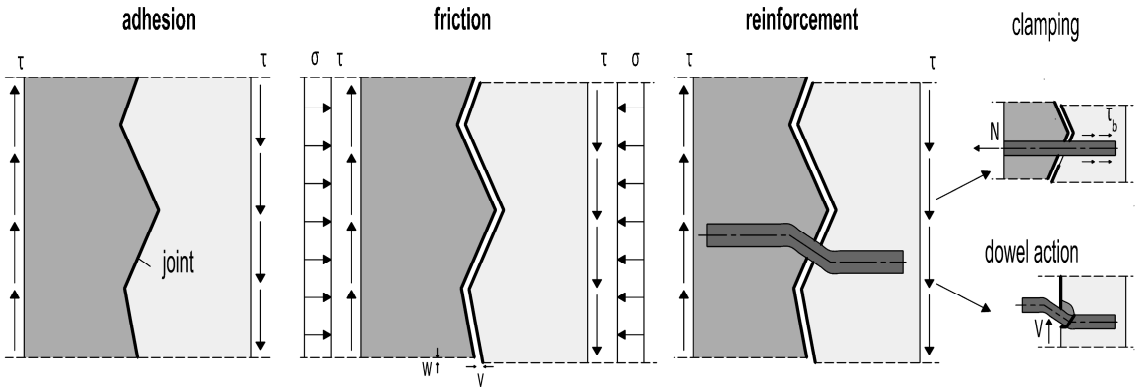


Figure 1. Load-carrying mechanisms in a joint exposed to shear [7].

For adhesion, physical bonds such as van der Waals forces in the form of hydrogen bonds and dipole-dipole bonds are involved. However, chemical bonds contribute to only a small part of the load transfer through ionic and covalent bonds compared to physical mechanisms such as mechanical interlock [8].

After adhesion is exceeded, a surface displacement occurs, which leads to interlocking due to surface roughness and the interaction of the aggregate grains with each other. In addition to the aggregate, this interlocking is also dependent on the reinforcement crossing the joint. The reinforcement resists the displacement of the crack surface, resulting in a clamping and dowel effect. In the case of the clamping effect, the forces are transferred from the joint to the interior of the component along the length of the reinforcement. In the case of the dowel effect, a combined load transfer takes place via the bending stress and the diagonal tension of the reinforcement [9].

The behavior of concrete joints has been extensively investigated in the past using steel reinforcement, e.g., [7,9–12]. A variation in roughness for unreinforced specimens was investigated by differentiating a surface that had been water-blasted or sand-blasted, as well as a surface that had been casted against formwork or casted without surface treatment [13]. According to the test results, the load bearing is dominated by friction and cohesion. Based on experiments using round steel dowels clamped in concrete, the embedment length upon which no changing in the ultimate load was stated equals 5·Ø [11]. A model of the pressure distribution along a reinforcement, assuming it behaves like a pole embedded in the ground, was provided first by [10]. For an embedment length of >6–8·Ø, concrete splintering instead of spalling occurs, and, additionally, a yielding of the reinforcement is observed. The model was modified by determining that the concrete section directly at the surface until the yielding zone plasticizes. Below this yielding zone the concrete does not form cracks [12]. The yielding zone can be found at 1·Ø [12].

The development of [14] was based on the discovery that reinforcements crossing a joint are only involved after a certain opening or displacement of the joint. The mechanisms for a slip smaller and greater than 0.05 mm, as well as a reinforcement ratio smaller or greater 0.05%, are distinguished by [14]. The case of a slip smaller than 0.05 mm, as well as a reinforcement smaller than 0.05%, is depicted in (1), consisting of the load-carrying behavior through adhesion and friction.

$$\tau_{Rd} = c_a \cdot f_{ctd} + \cdot\sigma_n \leq 0.5 \cdot \nu \cdot f_{cd} \quad (1)$$

With

c_a	Coefficient for adhesive bond;
f_{ctd}	Design tensile strength of concrete;
	Coefficient of friction;
σ_n	Stress due to external normal force;
ν	Reduction factor for shear strength of diagonal concrete strut;
f_{cd}	Design compressive strength of concrete.

When the slip exceeds 0.05 mm, the reinforcement participates in the load-bearing, and the resisting shear strength is depicted in (2) as in [14].

$$\tau_{Rd} = c_r \cdot f_{ck}^{\frac{1}{3}} + \cdot(\sigma_n + \rho \cdot \kappa_1 \cdot f_{yd}) + \kappa_2 \cdot \rho \cdot \sqrt{f_{yd} \cdot f_{cd}} \leq \beta_c \cdot \nu \cdot f_{cd} \quad (2)$$

With the formula symbols, in addition to the listing beforehand

c_r	Coefficient for adhesive bond for slip >0.05 mm;
f_{ck}	Characteristic compressive strength of concrete;
κ_1	Coefficient of efficiency for tensile force that can be activated in the reinforcement;
f_{yd}	f_{yd} Design tensile strength of steel;
κ_2	κ_2 Coefficient for flexural resistance of reinforcement (dowel action);
β_c	β_c Coefficient allowing for angle of diagonal concrete strut.

This article focuses on the strength of non-metallic bars perpendicular to their fiber orientation. Since non-metallic bars consist of pure fibers and a surrounding polymer impregnation, the material properties differ widely depending on the direction of loading. The load-carrying capacity perpendicular to the fiber orientation is examined in an experiment for a single bar in a uniaxial shear test and for the reinforcements embedded in concrete in a push-off test. The test series for the concrete joints analyzes the influence of the roughness of the joint, as well as the amount and type of reinforcement.

1.3. Novelty of the Test Setup

The presented test setups had not yet been used in the context of non-metallic reinforcement. The uniaxial shear test of a single bar was conducted inspired by [15] performing a ASTM D7617/D7617M [16] shear test on glass fiber-reinforced polymers with varying profiles. This test-setup was not adopted entirely since the blade pushing down on the reinforcement bar is surrounding it, which translates to stiff behavior from the steel compared to the soft behavior of concrete that exists in reality [17]. A reinforcing bar with a spiral sheathing as a profile had a greater load-bearing capacity than milling off material [15]; thus, both types of profiles were used in the presented test setup. In addition, carbon fiber-reinforced polymer bars (CFRPs) exhibited no recorded information on shear behavior; hence, this study guarantees new insights into the behavior of non-metallic reinforcements. Regarding the push-off test of reinforcement crossing a joint, first insights in the role of dowel action using CFRP textiles have been given. It was stated that dowel action in the shear transfer of FRP textile-reinforced members should not simply be negated [18]. The test setup used plates of two thicknesses, predefining a crack specified with and inducing a normal force. The predefinition of a crack in the presented test setup was executed by creating two joints (see Section 2.2), and the introduction of a normal force was avoided in order to exclude positive effects on the shear capacity (see Formulas (1) and (2)).

2. Materials and Methods

2.1. Materials

As for the reinforcement, two different types of bars were used. A yarn made of carbon fibers is helically twisted around the carbon core of the bar (CFRP). The glass bar profile (GFRP) is twisted as well, but it is achieved by milling out material (see Figure 2). The

nominal diameter is defined as the diameter where there is a completely circular cross section. Further properties from the technical data sheet can be found in Table 1.

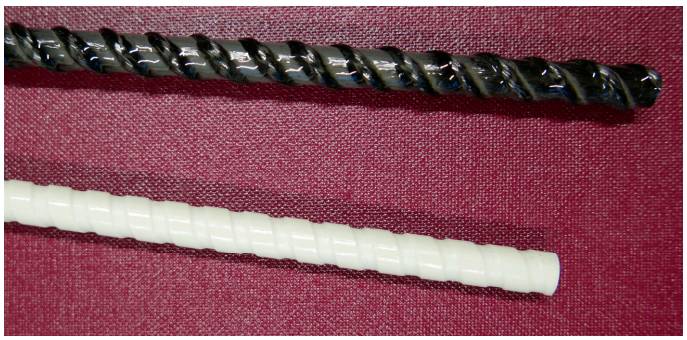


Figure 2. Detail of investigated reinforcement: carbon reinforcement—black: solidian REBAR D8-CCE; white: Schöck ComBAR, d = 8 mm.

Table 1. Properties from technical data sheet [19,20].

Properties	Unit	Carbon	Glass
Nominal diameter	mm	8	8
Ultimate tensile strength	N/mm^2	2100 [1]	1000
Ultimate strain	‰	15 [2]	7.4 [3]
Modulus of elasticity	N/mm^2	140,000 [4]	60,000 [5]
Fiber volume content	%	64	75
Nominal cross-sectional area	mm^2	50.3	50.3

[1] Characteristic short-time tensile strength regarding the nominal cross-sectional area. [2] Characteristic elongation at break. [3] Strain at Ultimate Limit State. [4] Average modulus of elasticity regarding nominal cross-sectional area. [5] Tension modulus of elasticity.

The concrete had a maximum aggregate size of 8 mm and the quantitative amount can be found in Table 2. According to DIN EN 206 [21], aggregate mixtures with an aggregate size smaller than 4 mm are classified as mortar. However, because of the relatively small aggregate size, the testing of the envisaged compressive strength was verified by prisms ($160 \times 40 \times 40$ mm^3) according to the standard test method for mortar DIN EN 1015-11 [22]. For each concrete batch, the compressive strength f_c was determined on three prisms, and the flexural tensile strength $f_{ct,fl}$ was determined on the two halves after each compression test on the day of testing (age 28 to 32 days). The average compressive strength of the concrete prisms was scaled to experiments of cube dimensions and resulted in 21.6 N/mm^2 [23].

Table 2. Mix design of the cementitious matrix for 1 m^3.

Component	Volume in dm^3	Density in kg/cm^3	Mass in kg
Water	199.81	1	199.81
Cement	105.37	3	316.1
Aggregate size 0–2 mm	379.87	2.63	999.05
Aggregate size 0–8 mm	297.21	2.63	781.66
Pore	20	-	-
Sum	1002.25 [1]	-	-

[1] The volume differs from 1000 cm^3 due to rounding.

2.2. General Procedure and Experimental Program

The present study differentiates between the uniaxial shear test and the push-off test. One main objective was to investigate the shear capacity of the samples in terms of the load-displacement characteristics. For the push-off test, the following parameters were varied:

- Roughness (smooth, rough: R_t = 1.41 mm);
- Ratio of reinforcement (one or two reinforcements crossing the joint);
- Type of reinforcement (carbon fiber-reinforced polymer, glass fiber-reinforced polymer).

Two reinforcements crossing the joint were only investigated for the smooth joint (geometry as in Figure 3). Three specimens were examined for the reinforced configuration, resulting in 18 reinforced and 6 unreinforced samples. Regarding the uniaxial shear test, 4 samples per reinforcement type, in total 8 samples were tested (Table 3). For each reinforcement type in the uniaxial shear test, only one sample was not tested until failure.

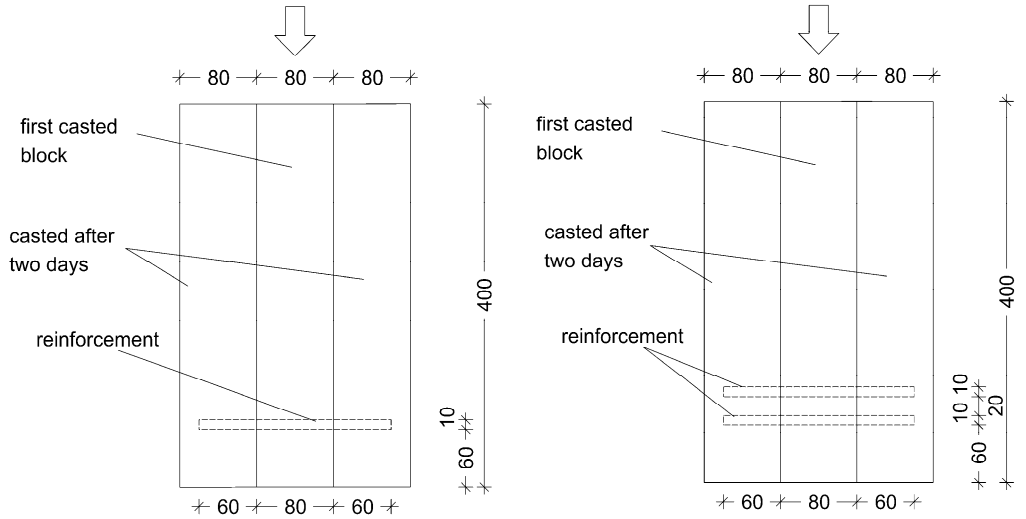


Figure 3. Specimen for the push-off test with: (**a**) one reinforcement crossing the joint; (**b**) two reinforcements crossing the joint.

Table 3. Number of experiments conducted for each test setup.

Uniaxial Shear Test		Push-Off Test			
Reinforcement Type	**Specimens**	**Reinforcement**	**Surface of the Joint**	**Reinforcements Crossing the Joint**	**Specimens**
Carbon	4	Carbon	Smooth	1	3
Glass	4		Smooth	2	3
			Rough	1	3
		Glass	Smooth	1	3
			Smooth	2	3
			Rough	1	3
		None	Smooth	-	3
			Rough	-	3
Total: 8 specimens		Total: 24 specimens			

2.3. Sample Preparation

The length of the bar for the uniaxial shear test was determined to 180 mm, respecting the conditions of ISO 10406-1 [24] being not more than 300 mm. The condition of the length being less than five times the shear plane interval could not be satisfied due to the restrictions of the load-charging equipment of the laboratory. The cutting was realized by using a diamond circular saw.

For the experiments of concrete joints, a three-layered specimen was built. The specimens used for this study were produced at the Otto-Mohr-Laboratorium (OML, Dresden, Germany). A formwork of sealed timber (340 × 280 × 90 mm^3) was prepared with three casting boxes. The inner part was casted with a fresh concrete consistency class of F3 according to DIN EN 12350-5 [24,25]. The specimens were roughened one day after casting by loosening the limiting formwork of the inner part. In order to roughen the generated surface evenly, the specimens were extracted from the formwork. The roughness was obtained by using water pressure. Determining the roughness coefficient R_t according to Kaufmann [26,27] as depicted in Figure 4a resulted in a roughness of 1.39 mm for the first batch and 1.42 mm for the second batch. A few hours after the roughening process, the concrete was embedded again in the formwork as in Figure 4b, casting the outer parts one day afterwards.



(**a**) (**b**)

Figure 4. Production of the samples with roughened concrete joints: (**a**) determining roughness depth; (**b**) formwork ready for second casting.

Due to the profile of the bars, especially for the carbon bars, the diameter of the hole in the formwork was not big enough to remove the formwork. Turning the formwork out along the profile resulted in stress being put on the young concrete, thus destroying it. Two specimens in the configuration of two reinforcements crossing the joint version had to be casted again. Probably, microcracks existed for the other specimens as well, albeit without being noted. Until the day of testing, the specimens remained in a climate chamber at a temperature of 20 °C with 65% relative humidity.

2.4. Test Setup and Instrumentation

2.4.1. Uniaxial Shear Test of Single Bar

Since the tests were of tentative nature, the test set-up was designed based on ISO 10406-1 [24]. The setup, as shown in Figure 5a, consisted of an upper blade (in this case, the machine charging equipment) exerting downward pressure on the bar and two lower blades supporting the bar. The demanded distance of the two lower blades of 50 mm could not be guaranteed by the load application of the testing machine at the Otto-Mohr-Laboratorium (OML) with 60 mm.

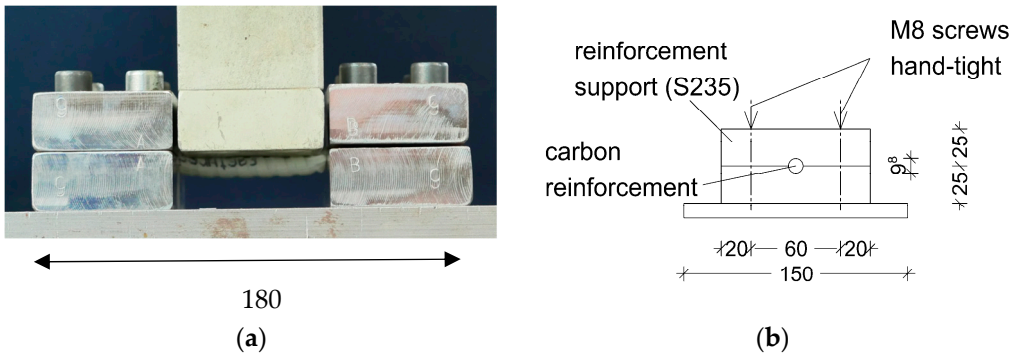


Figure 5. Uniaxial shear test: (**a**) front view of test-setup; (**b**) side view scheme of test-setup (dimensions in mm).

The upper blade was not adapted to the diameter of the tested bar and a plane surface, whereas the halves of the lower blades were drilled with the diameter according to the tested reinforcement type. In order to prevent the lower blade halves from opening up, four screws assured the position between two halves and the position on the test machine (Figure 5b). The setup was screwed to the frame of the testing machine with a compressive load capacity of 250 kN.

The load was applied in a displacement-controlled manner at a loading rate of 1 mm/min until failure for three specimens and until extreme bending for one specimen. Before starting the test, a force of 100 N was applied in order to align the calotte of the test setup.

2.4.2. Push-off Test of Reinforcement Crossing a Joint

The specimen with three concrete parts was tested while standing on metal blocks, allowing the inner part to move downward without any hindrance. The aim of the test setup was to determine the force that could be transferred by the reinforcement. If the specimen is clamped on both sides, the normal force created while doing so contributes to the resisting force of the joint. In order to avoid this effect, steel profiles were placed on both sides, with distance to the specimen only for the case of falling (Figure 6).

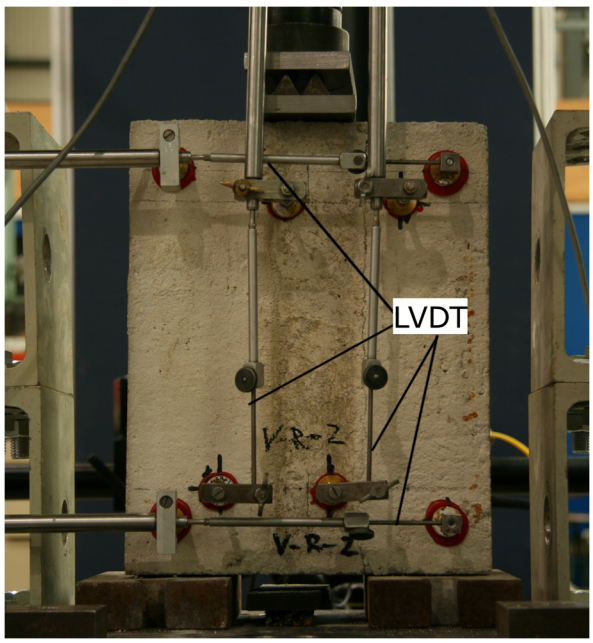


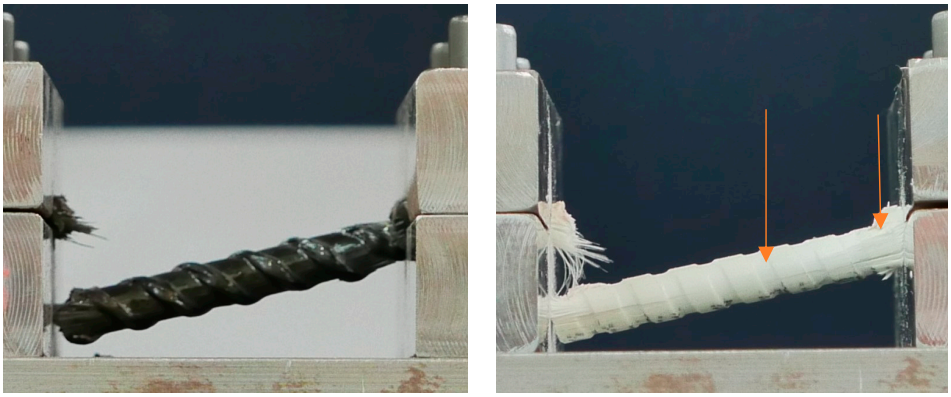
Figure 6. Push-off test setup of reinforcement crossing a joint.

The load was applied in a displacement-controlled manner at a loading rate of 0.5 mm/min until the crushing of the concrete around the reinforcement bar. A force of 200 N was applied in order to align the load from the metal plates to the specimen. During the experiments, the machine force F, as well as the vertical machine displacement w, were measured. In order to monitor the horizontal opening of the joints, one inductive displacement sensor (linear variable differential transformer—LVDT) was installed on the upper part, and one was installed on the lower part beneath the reinforcement bar. The displacement of the joints was determined with two vertical inductive displacement sensors, one in each joint.

3. Results and Discussion

3.1. Uniaxial Shear Test Result of Single Bar

The experiments were conducted in order to deliver a better understanding of the shear failure of non-metallic reinforcement. Figure 7 shows photographs of the failure pattern. All specimens failed on the left lower blade after a displacement of over 6.7 mm regarding the carbon reinforcement and 5.3 mm for the glass reinforcement. Until the failure bending occurred in the middle of the bar (see Figure 5a). Some fibers close to the support are detached and a crack in the surface propagates widely from the joint away further into the middle of the reinforcement bar, as it can be seen in Figure 7b (orange arrows).



(**a**) (**b**)

Figure 7. Uniaxial shear test after failure: (**a**) carbon reinforcement; (**b**) glass reinforcement.

Regarding the tensile strength, one can note that the characteristic short-time tensile strength of carbon reinforcement is higher than the one of glass reinforcement (2100 N/mm^2 > 1000 N/mm^2 [19,20,28]). This tendency was also observed in the shear force, as shown in Figure 8. In addition, the curve trend varies from parabolic for the carbon bars to parabolic with two drops at a displacement of approximately 1 and 2 mm for the glass bar. One offered explanation is the failure of the surrounding matrix, which is scattered during the test of all the carbon bars and two times significantly for the glass bars.

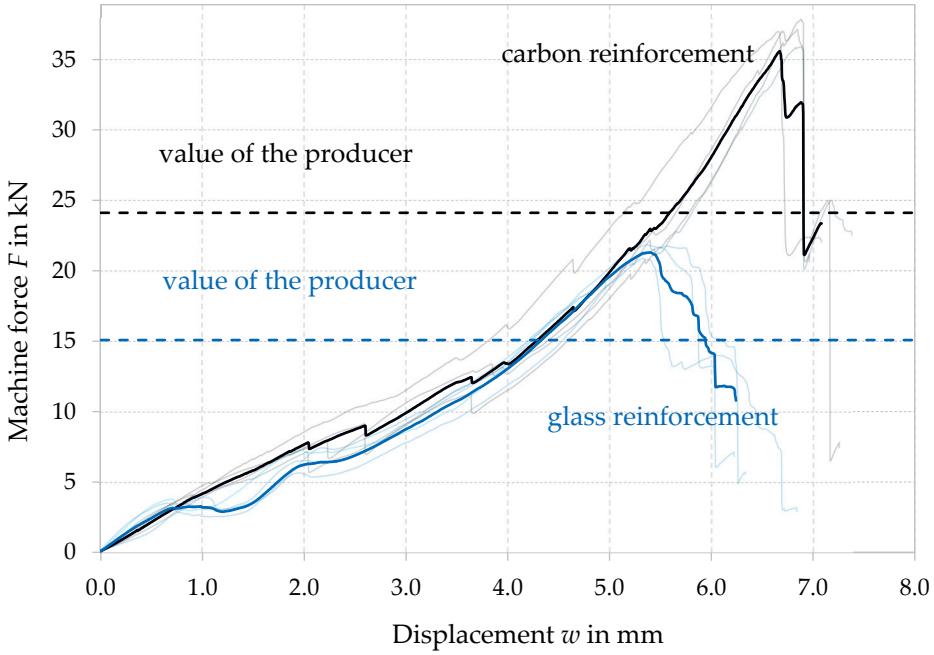


Figure 8. Force-machine displacement diagram for the uniaxial shear test comparing carbon reinforcement with glass reinforcement. The highlighted curve represents the average value.

The shear strength (τ_s) can be calculated with the aid of dividing the ultimate force (P_s) by two times the cross section according (A) to ISO 10406-1 [20] as follows:

$$\tau_s = \frac{P_s}{2 \cdot A}$$

On average, the samples achieved an average shear strength of 366.5 N/mm^2 regarding the carbon reinforcement and 213.7 N/mm^2 for the glass reinforcement according to Table 3. The values for the shear strengths of the producers were smaller than the experimentally determined values. The producer of the carbon reinforcement removed the profiling prior to testing. As the nominal cross section stays the same, it translates to a lower ultimate force in the test of the producer compared to our own obtained ultimate force. The profiling, therefore, led to higher ultimate forces and should be taken into account. According to [19], the profile was removed in order to provide replicability, and the values were rounded down, ensuring safety in the dimensioning. The blade in the shear test of the carbon reinforcement producer surrounded the reinforcement, whereas the blade in the here presented test setup pushed only onto the surface of the reinforcement. This reasoning explains the ratio of the producers' value to the average experimentally developed values of 65% for the carbon reinforcement and 70% regarding the glass reinforcement. Further investigation showed that a higher value for the rib inclination angle suggests a greater tendency towards splitting [29]. Comparing the used reinforcements, this translates to a greater tendency towards splitting for the glass fiber-reinforced polymer than for the carbon fiber-reinforced polymer. Figure 7 confirms that GFRPs have greater splitting than CFRPs. The details of the test results are listed in Table 4.

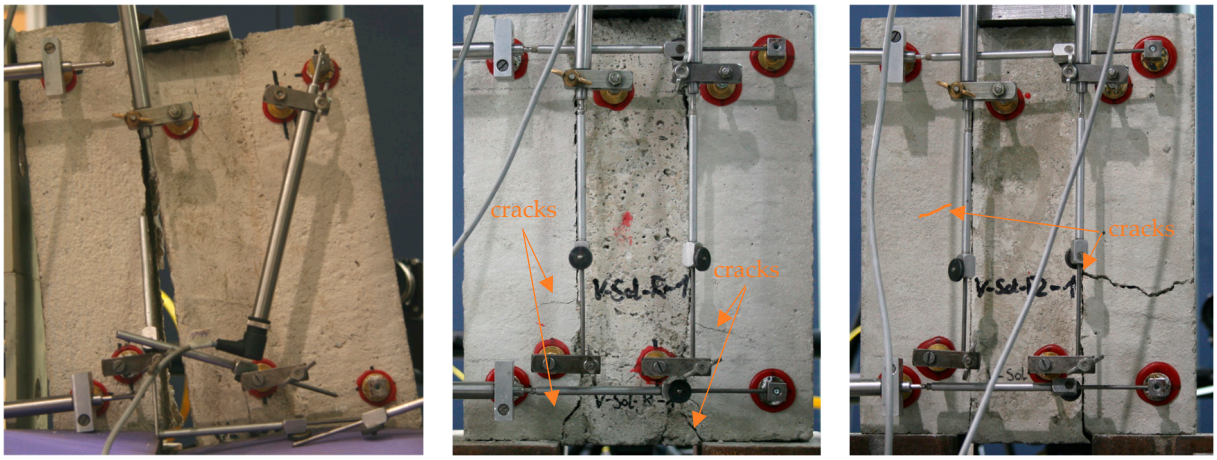
Table 4. Uniaxial shear test results.

	Carbon Reinforcement			Glass Reinforcement		
	P_s	w	τ_s	P_s	w	τ_s
Sample No.	**in kN**	**in mm**	**in N/mm²**	**in kN**	**in mm**	**in N/mm²**
1	36.9	6.7	366.8	21.8	5.6	216.7
2	35.9	6.9	356.9	21.8	5.4	217.7
3	37.8	6.9	375.7	20.9	5.3	207.8
Average value	36.9	6.8	366.5	21.5	5.4	213.7
Variation	0.9	0.01	89.3	0.3	0.02	26.7
Standard deviation	1.0	0.1	9.4	0.5	0.2	5.2
Average transversal shear strength (producer value)		240 N/mm²				150 N/mm²

3.2. Push-off Test Results of Reinforcements Crossing a Joint

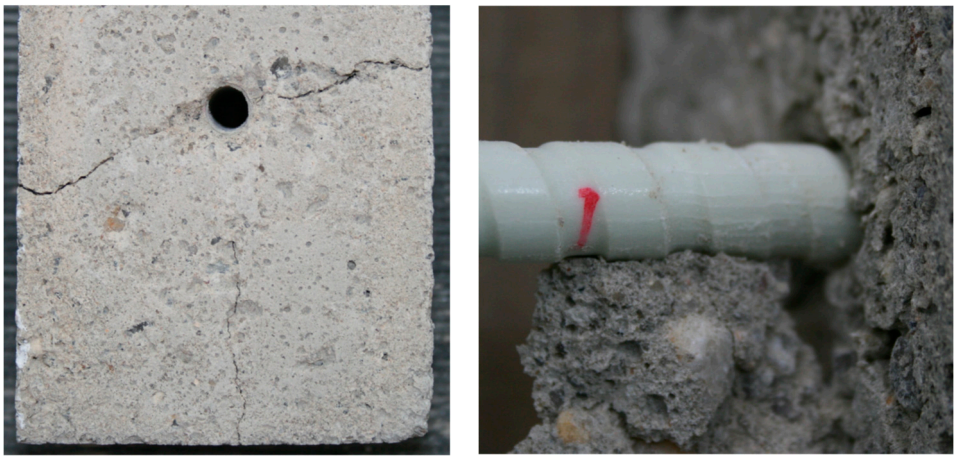
With 6 unreinforced specimens and nine specimens for each reinforcement type, the shear behavior of concrete joints was assessed. Figure 9 shows a selection of possible failure patterns of the specimens. The specimens with no reinforcement failed brittle, and the entire specimen tilted towards one side (Figure 9a). The rough surface of the joint created small concrete spalling along the joint. Comparing the specimen where there was one reinforcement crossing the joint to two reinforcements, it was noted that the failure of the concrete was also brittle, but the three parts of the specimens were held together by the reinforcement. In addition, cracks occurred above the reinforcement (Figure 9b,c orange arrows) and propagated from the joint towards the end of the reinforcement. The formation of the crack coincided with the peak load, as in [18]. The experiments for the specimens with two reinforcements crossing the joint were conducted until a machine displacement of at least 5.6 mm was achieved, resulting in crack widths of 2.5 mm and even separating the concrete blocks above the reinforcement from the part below. This enabled an analysis of the reinforcement embedded in the concrete.

In order to analyze the torsion of the reinforcement and the crack in the cross section, the three parts of the specimens were separated from each other. The cracks in the concrete are caused by exceeding the concrete tension force, resulting in a crack. The cracks begin on the surface and disperse toward the reinforcement, as shown in Figure 10a. The formation of the cracks results from the destroyed adhesive bond along the joint. The reinforcement that crosses the joint is therefore the most contributing component for transferring the force of the inner concrete part to the two outer concrete parts. The vertical force on the test specimen is transformed into a horizontal force by the reinforcement. The surrounding concrete, thus, receives a tensile force, which the concrete withstands less effectively than a compressive force. The appearance of longitudinal cracks in the plane of the reinforcement is confirmed by [18].



(**a**) (**b**) (**c**)

Figure 9. Push-off test: (**a**) unreinforced specimen with rough joint; (**b**) carbon-reinforced specimen (one reinforcement crossing the joint and rough joint); (**c**) carbon-reinforced specimen (two reinforcements crossing the joint and smooth joint).



(**a**) (**b**)

Figure 10. Details of failure for reinforcements embedded in concrete: (**a**) top view of a side concrete block with reinforcement (removed for photo); (**b**) damaged surface of glass reinforcement near the shear plane.

That the reinforcement has been exposed to shear is depicted in Figure 10b. The type of crack along the reinforcement near the shear plane resembles the crack obtained during the uniaxial shear test of the single bar (Figure 7b), but the cracks in Figure 10b are only in the surface of the reinforcement.

The brittle behavior of specimens without reinforcements is illustrated in a force-displacement diagram in Figure 11a,b. Roughening the surface does not impact the adhesion failure, as the curves have a significant drop as well. However, the ultimate force until failure of the joint is higher for the roughened surface. There is no drop near to 0 N for the reinforced specimens in Figure 11a, contrary to the unreinforced specimens. This cannot be shown for all unreinforced specimens because the machine stops the test when the force drops 95%. In Figure 11a, the ultimate force for the reinforced joint for two out of three specimens is slightly above that of the unreinforced joint. In Figure 11b, the opposite can be stated. The finding is unexpected, taking into account the fact that roughness typically results in a greater surface being available for adhesion forces, thus increasing the resistance to shear displacement. Comparing the calculation of resisting shear stress in joints according to [14], the rough surface has a higher resistance, since the

design value of the adhesive bond (c_a in Equation (1)) is greater. One explanation for the test result could be that the reinforcement crossing the joint reduces the surface available for adhesion forces. A second explanation is offered by the erased material of the rough surface due to transport and reassembly, thus smoothening the joint before the second casting can take place. Another difference between the two diagrams is the behavior after the concrete joint fails. In Figure 11b, the rough surface with its hilly structure on a microscopic level becomes smoother with the further displacement of the joint. Hence, the force diminishes only slowly after the force drop. The contribution of reinforcement to the load-carrying capacity is evident in Figure 11a, which shows a new local maximum after an average machine path of 1.5 mm.

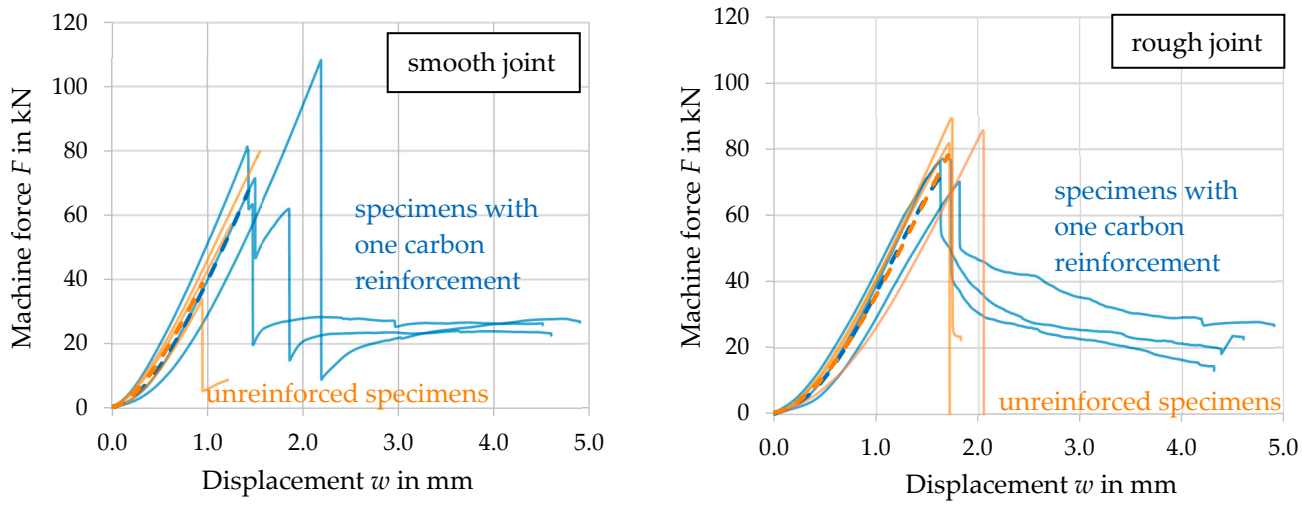


Figure 11. Force-displacement diagram comparing unreinforced and carbon-reinforced joints (dash line represents average value): (**a**) for smooth joints; (**b**) for rough joints.

The glass reinforced specimens achieved smaller ultimate loads compared to the carbon-reinforced specimens regarding the smooth joint for one and two reinforcements crossing the joint (see Table 5). This is not the case for the rough joint, where the glass reinforcement has a slightly higher ultimate load than the carbon fiber crossing the joint. The failure behavior is similar to that of the carbon-reinforced specimens, even though two significant drops in the curve take place in the case of the glass fiber reinforcement (Figure 12 light green line). This could be explained by an asymmetrical arrangement in the test machine, thus resulting in one joint being more loaded than the other, and as a result, one joint fails before to the other. A significant increase in the ultimate force is stated for two reinforcements crossing the joint (Figure 12, dark green line). This applies to both types of reinforcement. In addition, a new local maximum in the curve appears after the concrete failure of the joint. The local maximum of the highest curve represents an exception, as the machine recorded the real force of the reinforcement representing a resistance only after a short delay. The ultimate force for the specimens with two reinforcements crossing the joint could be even higher if the holes in the formwork are significantly greater and do not lead to the preliminary damage of the specimens, as described in Section 2.3.

Table 5. Push-off test results of reinforcements crossing a joint (ultimate force P_s in kN).

	Unreinforced		Carbon Reinforcement			Glass Reinforcement		
Joint Surface	**Smooth**	**Rough**	**Smooth**		**Rough**	**Smooth**		**Rough**
No. of reinforcements	0	0	1	2	1	1	2	1
Sample 1	57	81.7	108.1	92.6	70	36.8	74	76.2
Sample 2	79.7	85.5	81.2	109.5	76.9	60.1	92.2	68.5
Sample 3	33.7	89.2	71.4	62.3	75.9	64	56.2	82.9
Average value	56.8	85.5	86.9	88.1	74.3	53.6	74.1	75.9
Variation	529	14.1	361.1	571.9	13.9	216.3	324	51.9
Standard deviation	23	3.8	19	23.9	3.7	14.7	18	7.2



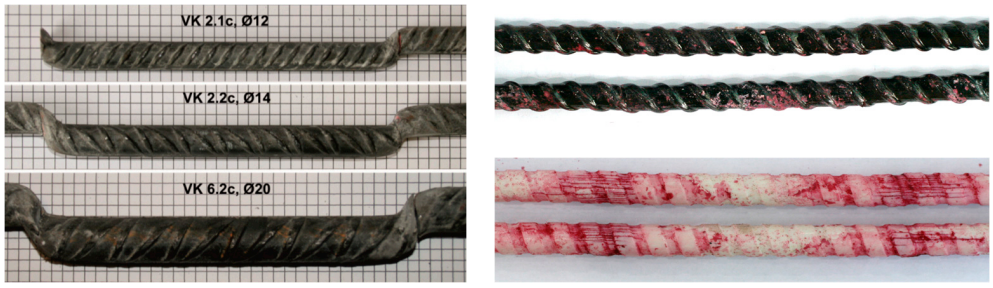
Figure 12. Force-displacement diagram comparing two glass reinforcements with one reinforcement crossing the joint and unreinforced specimens.

On average, the unreinforced samples with smooth joints achieved an average ultimate load of 56.8 kN, compared to 85.5 kN for the unreinforced samples with rough joints. A significant standard deviation was stated for the unreinforced specimens with smooth joints. Concerning the specimens with carbon reinforcement, the ultimate load was 86.9 kN for the smooth joint and 74.3 kN for the rough joint. Comparing these values with the glass fiber reinforcement, one can note that the ultimate load for the smooth joint with 53.6 kN was higher for the carbon-reinforced joints. Regarding the rough joint, the ultimate load for joints with glass rebars was slightly greater at 75.9 kN compared to carbon-reinforced joints. Throughout the smooth joints, a high standard deviation was noted. This can be explained in part by the inhomogeneity of the concrete joint. The details of the test results are listed in Table 5.

The findings correlate with the results of other authors. The ultimate shear force is a function of the reinforcement ratio, according to [30]. The shear force was determined by reinforcing the joint of two L-formed specimens with glass fiber-reinforced polymers (GFRPs). The test setup of two concrete blocks, casted one after the other and reinforcing the joint with GFRPs, showed that with a rising number of reinforcements crossing the joint, the bearing capacity increases.

A qualitative analysis of the bending behavior of steel, carbon and glass bars is shown in Figure 13. Steel reinforcement develops a plastic hinge at a distance of approximately

one time the diameter from the joint (see Figure 13a) [7]. Comparing the tested non-metallic reinforcement as in Figure 13b, it can be observed that there is a slight deformation, for the carbon bar, and there are cracks in the profiling of the glass bar. In order to make the cracks visible, a red color spray was used. The photographs, as in Figure 13b, are the result of a different modulus of elasticity. The carbon fiber has a higher modulus of elasticity in the longitudinal direction, thus resulting in a greater resistance against cracks in the profiling. There were also some small fissures that could not be made visible using coloring spray.



(**a**) (**b**)

Figure 13. Details of failure for reinforcements crossing a joint: (**a**) steel reinforcement [7]; (**b**) carbon reinforcement (top) and glass reinforcement (bottom) for specimens with two reinforcements crossing the joint.

4. Conclusions

This paper investigated shear loads for single non-metallic bars and concrete specimens with non-metallic reinforcements crossing two joints. Reinforcement bars as carbon fiber-reinforced polymers (CFRPs) and glass fiber-reinforced polymers (GFRPs) with the same diameter have been used. The contribution of non-metallic reinforcement should not be negated, as in the German DAfStb-guideline for non-metallic reinforcement [6]. This paper gives a first insight into the shear capacity of non-metallic reinforcement.

The main conclusions are as follows:

1. Shear tests on single bars revealed shear strengths that exceeded manufacturer-provided values, attributed to a different test setup and the unmodified profile of the reinforcement bars. Initially, only force and machine displacement were recorded; future research will include strain measurements in the longitudinal direction, circumferential crack development and modifications to the test setup as per the ASTM D7617/D7617M standards [16].
2. Push-off tests of reinforcements crossing the joints in concrete specimens showed that the behavior after exceeding adhesion was ductile in comparison to joints without reinforcements, where the behavior was brittle.
    a. A drop from, on average, 87 kN to 16 kN was stated for the specimens with a smooth joint and one bar of CFRPs crossing the joint. A drop from 53 kN to 25 kN concerning one bar of GFRPs crossing the smooth joint existed compared to a drop from, on average 57 kN to 0 kN, for a specimen with a smooth joint and no reinforcement crossing the joint.
    b. Specimens with two reinforcements crossing the joint exhibited a higher ultimate shear force than those with a single reinforcement. The factor for the GFRP reinforcement crossing the joint was 1.38 on average. The CFRPs showed only a small factor of 1.01.
    c. CFRP-reinforced specimens demonstrated higher ultimate forces than GFRP-reinforced ones, as the ultimate tensile strength of the CFRP bars was 2.1 higher than those for the GFRP bars.
    d. Significant standard deviations highlighted the need for larger population size in future tests.

3. Further research should explore varying reinforcement diameters, the compressive strength of concrete, joint roughness and the reinforcement orientation (e.g., embedding at a 45° angle). A comprehensive examination of shear transfer mechanisms is essential for developing a robust assessment approach through additional modeling.

Author Contributions: Conceptualization, L.Z. and E.B.; methodology, L.Z. and E.B.; formal analysis, L.Z.; investigation, L.Z.; resources, S.M., D.S. and E.B.; writing—original draft preparation, L.Z.; writing—review and editing, L.Z., E.B. and D.S.; visualization, L.Z.; supervision, S.M. and E.B.; project administration, E.B. All authors have read and agreed to the published version of the manuscript.

Funding: This research was funded by the Federal Ministry of Education and Research of Germany via grant number 03LB3007C EDISON-rCF short fot he german project name "Verbundvorhaben: EDISON-rCF – Energieeffizientes werkstoffgerechtes Recycling von CFK durch einen innovativen Solvolyseprozess sowie die Entwicklung und Herstellung neuartiger quasiunidirektionaler Halbzeuge; Teilvorhaben: Bewehrungsentwicklung und Charakterisierung stabförmiger und flächiger Halbzeuge". Project period was from 2021 to 2023.

Data Availability Statement: The data presented in this study are available upon reasonable request from the corresponding author. The data are not publicly available due to this work being part of an ongoing study.

Acknowledgments: The authors would like to thank the staff of the OML for the support extended during the experimental works carried out at the laboratory.

Conflicts of Interest: The authors declare no conflict of interest.

References

1. Organisation Baunetzwissen Betonherstellung und Klimaschutz. Available online: https://www.baunetzwissen.de/beton/fachwissen/herstellung/betonherstellung-und-klimaschutz-7229519 (accessed on 21 February 2024).
2. Gouda, M.G.; Mohamed, H.M.; Manalo, A.C.; Benmokrane, B. Experimental investigation of concentrically and eccentrically loaded circular hollow concrete columns reinforced with GFRP bars and spirals. *Eng. Struct.* **2023**, *277*, 115442. [CrossRef]
3. Frenzel, M.; Baumgärtel, E.; Marx, S.; Curbach, M. The Cracking and Tensile-Load-Bearing Behaviour of Concrete Reinforced with Sanded Carbon Grids. *Buildings* **2023**, *13*, 2652. [CrossRef]
4. Frenzel, M.; Curbach, M. Shear strength of concrete interfaces with infra-lightweight and foam concrete. *Struct. Concr.* **2018**, *19*, 269–283. [CrossRef]
5. Wagner, J.; Curbach, M. Carbonstäbe im Bauwesen. *Beton-Und Stahlbetonbau* **2021**, *116*, 587–593. [CrossRef]
6. German Committee for Reinforced Concrete (DAfStb). *DAfStb-Richtlinie—Betonbauteile mit Nichtmetallischer Bewehrung: 2024-01*; Beuth Verlag GmbH: Berlin/Heidelberg, Germany, 2024.
7. Wingenfeld, D.R. Fügetechnische Konstruktionslösungen für Bauteile aus Ultrahochfestem Beton (UHPC). Ph.D. Dissertation, Technischen Universität München, Munich, Germany, 2013.
8. Lenz, P. Beton-Beton-Verbund. Ph.D. Dissertation, Technische Universität München, Munich, Germany, 2012. Available online: https://mediatum.ub.tum.de/604993?query=Potential+f%C3%BCr+Schubfugen+Lenz&show_id=1106588&srcnodeid=604993 (accessed on 7 March 2023).
9. Paulay, T.; Park, R.; Phillips, M.H. Horizontal Construction Joints in Cast-In-Place Reinforced Concrete. *Int. Concr. Abstr. Portal* **1974**, *42*, 599–616. Available online: https://www.concrete.org/publications/internationalconcreteabstractsportal/m/details/id/17303 (accessed on 7 March 2023).
10. Vintzēleou, E.N.; Tassios, T.P. Behavior of Dowels Under Cyclic Deformations. *ACI Struct. J.* **1987**, *84*, 18–30. [CrossRef]
11. Utescher, G.; Herrmann, H. *Versuche zur Ermittlung der Tragfähigkeit in Beton Eingespannter Rundstahldollen aus Nichtrostendem Austenititschem Stahl*; Deutscher Ausschuss für Stahlbeton: Berlin/Heidelberg, Germany, 1983; Volume 346, pp. 49–104.
12. Randl, N. Untersuchungen zur Kraftübertragung Zwischen Alt- und Neubeton bei Unterschiedlichen Fugenrauhigkeiten. Dissertation, Universität Innsbruck, Innsbruck, Austria, 2000. Available online: https://bibsearch.uibk.ac.at/AC02287162 (accessed on 27 June 2023).
13. Reinecke, R. Haftverbund und Rissverzahnung in Unbewehrten Betonschubfugen. Ph.D. Dissertation, Technische Universität München, Munich, Germany, 2002. Available online: https://mediatum.ub.tum.de/node?id=601067 (accessed on 23 June 2024).
14. Randl, N. Design recommendations for interface shear transfer in fib Model Code 2010. *Struct. Concr.* **2013**, *14*, 230–241. [CrossRef]
15. Gentry, R.; Bakis, C.; Harries, K.; Brown, J.; Prota, A.; Parretti, R. Development of ASTM test methods for FRP composite materials: Overview and transverse shear. In Proceedings of the 6th International Conference on FRP Composites in Civil Engineering, CICE 2012, Rome, Italy, 13–15 June 2012.
16. *ASTM D7617*; Test Method for Transverse Shear Strength of Fiber-reinforced Polymer Matrix Composite Bars. ASTM International: West Conshohocken, PA, USA, 2017.

17. Weber, A. Useful Shear Tests for FRP Dowels and Rebars. Available online: https://www.researchgate.net/publication/335136655_USEFUL_SHEAR_TESTS_FOR_FRP_DOWELS_AND_REBARS (accessed on 18 January 2024).
18. Bielak, J. On the role of dowel action in shear transfer of CFRP textile-reinforced concrete slabs. *Compos. Struct.* **2023**, *311*, 116812. [CrossRef]
19. Solidian. Technical Product Data Sheet—Solidian-REBAR-Dxx-CCE. 2023. Available online: https://solidian.com/wp-content/uploads/solidian-REBAR-Dxx-CCE-Technical-Product-Data-Sheets-v2303.pdf (accessed on 10 April 2024).
20. Schöck Bauteile. Technische Information Schöck Combar. 2019. Available online: https://www.schoeck.com/view/7725/Technische_Information_Schoeck_Combar___7725__.pdf/de (accessed on 21 May 2023).
21. *DIN EN 206*; Beton—Festlegung, Eigenschaften, Herstellung, Konformität. Beuth Verlag GmbH: Berlin/Heidelberg, Germany, 2021.
22. *DIN EN 1015-11:2020*; Prüfverfahren für Mörtel für Mauerwerk—Bestimmung der Biegezug- und Druckfestigkeit von Festmörtel. Beuth Verlag GmbH: Berlin/Heidelberg, Germany, 2020.
23. *DIN EN 206-1/DIN 1045-2*; Bestimmung von Korrelationen zwischen Würfel- und Prismendruckfestigkeit von Vergussmörteln für die Einordnung in Druckfestigkeitsklassen nach. Fraunhofer IRB Verlag: Stuttgart, Germany, 2009. Available online: https://www.irbnet.de/daten/rswb/08119015371.pdf (accessed on 23 April 2024).
24. *ISO 10406-1:2015*; Fibre-Reinforced Polymer (FRP) Reinforcement of Concrete—Test Methods—Part 1: FRP Bars and Grids. Beuth Verlag GmbH: Berlin/Heidelberg, Germany, 2015.
25. *DIN EN 12350-5:2019-09*; Prüfung von Frischbeton—Ausbreitmaß. Beuth Verlag GmbH: Berlin/Heidelberg, Germany, 2019.
26. *DIN EN 13036-1:2010-10*; Oberflächeneigenschaften von Straßen und Flugplätzen_-Prüfverfahren_-Teil_1: Messung der Makrotexturtiefe der Fahrbahnoberfläche mit Hilfe eines volumetrischen Verfahrens. Beuth Verlag GmbH: Berlin/Heidelberg, Germany, 2010.
27. *DIN EN 1766:2017-05*; Produkte und Systeme für den Schutz und die Instandsetzung von Betontragwerken_-Prüfverfahren_-Referenzbetone für Prüfungen. Beuth Verlag GmbH: Berlin/Heidelberg, Germany, 2017.
28. Bochmann, J. Carbonbeton unter Einaxialer Druckbeanspruchung. Ph.D. Dissertation, Technische Universität Dresden, Fakultät Bauingenieurwesen, Dresden, Germany, 2019.
29. Luo, Y.; Liao, P.; Pan, R.; Zou, J.; Zhou, X. Effect of bar diameter on bond performance of helically ribbed GFRP bar to UHPC. *J. Build. Eng.* **2024**, *91*, 109577. [CrossRef]
30. Alkatan, J. FRP Shear Transfer Reinforcement for Composite Concrete Construction. Master's Thesis, University of Windsor, Windsor, ON, Canada, 2016. Available online: https://scholar.uwindsor.ca/etd/5792 (accessed on 18 June 2023).

Disclaimer/Publisher's Note: The statements, opinions and data contained in all publications are solely those of the individual author(s) and contributor(s) and not of MDPI and/or the editor(s). MDPI and/or the editor(s) disclaim responsibility for any injury to people or property resulting from any ideas, methods, instructions or products referred to in the content.